



HAL
open science

Challenges in attributing the 2022 Australian rain bombs to climate change

Camille Cadiou, Nemo Malhomme, Robin Noyelle, Davide Faranda

► To cite this version:

Camille Cadiou, Nemo Malhomme, Robin Noyelle, Davide Faranda. Challenges in attributing the 2022 Australian rain bombs to climate change. 2022. hal-03722233v1

HAL Id: hal-03722233

<https://hal.science/hal-03722233v1>

Preprint submitted on 13 Jul 2022 (v1), last revised 25 Oct 2022 (v2)

HAL is a multi-disciplinary open access archive for the deposit and dissemination of scientific research documents, whether they are published or not. The documents may come from teaching and research institutions in France or abroad, or from public or private research centers.

L'archive ouverte pluridisciplinaire **HAL**, est destinée au dépôt et à la diffusion de documents scientifiques de niveau recherche, publiés ou non, émanant des établissements d'enseignement et de recherche français ou étrangers, des laboratoires publics ou privés.

Challenges in attributing the 2022 Australian rain bombs to climate change

Camille Cadiou^{1†}, Nemo Malhomme^{1†}, Robin Noyelle^{1†}
and Davide Faranda^{1,2,3*}

¹Laboratoire des Sciences du Climat et de l'Environnement,
LSCE/IPSL, CEA-CNRS-UVSQ, Université Paris-Saclay,
Gif-sur-Yvette, 91191, France.

²London Mathematical Laboratory, 8 Margravine Gardens
London, W6 8RH, London, United Kingdom.

³LMD/IPSL, Ecole Normale Supérieure, PSL research University,
Paris, France.

*Corresponding author(s). E-mail(s): davide.faranda@cea.fr;
Contributing authors: camille.cadiou@lsce.ipsl.fr;
nemo.malhomme@lsce.ipsl.fr; robin.noyelle@lsce.ipsl.fr;

[†]These authors contributed equally to this work.

Abstract

In February and March 2022, the eastern coast of Australia recorded unprecedented amount of precipitation with extended floods and damages to properties amounting at least to AUD 2.3 billions. In this paper we use both reanalysis and observations to perform a statistical and dynamical attribution of this precipitation event to climate change. We define 1948-1977 as the counterfactual period and 1990-2019 as the factual one. The statistical attribution is based on fitting the generalized extreme value distribution for 3-days precipitation annual maxima for the two periods, while the dynamical attribution aims at looking at the recurrence properties of sea-level pressure and geopotential height patterns in both periods. We find that the dynamics of the event consists in an unprecedented combination of several factors: a tropical atmospheric river, the presence of the Coral low and a blocking anticyclone offshore Eastern Australia. Our main finding is that no clear attribution statements can be made, because of its unprecedented

nature, the lack of long high quality available data and the dependence of the results on the La Nina phase of El Nino Southern Oscillation.

Keywords: Climate Change, Extreme Precipitation, Attribution, Australia

1 Introduction

In the latest IPCC report (Masson-Delmotte et al, 2021), researchers confirm the role that human activity plays in the climate upheavals of recent decades. The scientists also hypothesize possible future scenarios and confirm the role of climate change on the frequency and intensity of extreme weather events that we experience today. The IPCC scientists warn in particular about the effects that climate change is having on the water cycle. Studies have shown that rising temperatures are leading to more intense rainfall, flooding but also to more severe droughts (Cook et al, 2018) in some regions of the world. The distribution, frequency and intensity of precipitations are changing significantly across the globe, especially in subtropical regions accustomed to monsoons (Douvillle et al, 2021). In the 21st century, coastal areas are already experiencing and will increasingly experience flooding due to heavy precipitation and sea level rise (Wilby and Keenan, 2012). Flooding from rising seas, which was only occasional a few decades ago, could occur every year by the end of the century (Hirabayashi et al, 2013).

Australian average temperatures have risen by 1.44°C since 1910, according to the recent study by Grainger et al (2022), who recall the proximity of the actual values to that of the Paris climate agreement, whose aim is to contain the rise in temperatures to 1.5°C compared to the pre-industrial era. The oceans surrounding the continent have also warmed by an average of one degree over the same period, leading to acidification and more frequent marine heat waves. Half of the corals in Australia's Great Barrier Reef have died since 1995 because of this rise in water temperature (Wolff et al, 2018; Holland et al, 2020). Few studies predict that sea levels will rise in line with international forecasts while tropical cyclones will be more intense (Church et al, 2006; Woodruff et al, 2013; Church et al, 2017). Other authors have also pointed out that rainfall has decreased in southwestern Australia as well as in the fire-ravaged southeast, even as it is more in the north, which has been hit by major floods and destructive cyclones in recent years (Dey et al, 2019; Abram et al, 2021).

If climate change projections for Australia are worrying, the country is already experiencing severe extreme weather events. Indeed, climate change has already taken its toll on Australia (Head et al, 2014; Abram et al, 2021; Canadell et al, 2021), which has been hit by fires, drought and intense cyclones. In 2019-2020 the country was already ravaged by wildfires of exceptional proportions after experiencing the hottest and driest year on record (Borchers Arriagada et al, 2020; Jetten et al, 2021). The fires destroyed

73 an area almost the size of the United Kingdom, killed several people and killed
74 or displaced nearly three billion animals, costing the Australian economy about
75 7 billion AUD (Filkov et al, 2020). In the current 2022 year, both high and low
76 temperature records have been broken in Australia. On one hand, the 13/01
77 The coastal town of Onslow reached an unprecedented 50.7°C, the warmest
78 temperature ever recorded in Australia for sixty-two years (The Guardian,
79 2022). On the other hand, on the 02/06, at the Thredbo Top weather station
80 the temperature reached -6.9°C and historic snowfalls for this time of year (The
81 New Daily, 2022). Future projections of climate-related disasters for the coastal
82 areas as well as the vast island-continent report an increasing risk of extreme
83 events capable of heavily damaging natural ecosystems and impact health and
84 agriculture (Hobday et al, 2018; Dey et al, 2019; Ukkola et al, 2020).

85 Here we will focus on the extreme precipitation event which occurred from
86 the last week of February to mid-March 2022, in the eastern coast of Aus-
87 tralia. 345mm of rain were recorded at Brisbane on the 28th of February. The
88 precipitations met soils already close to saturation from the recent rains in
89 the end of 2021. This led to severe and enduring floodings during the month
90 of March. This event caused 22 recorded casualties, rendered uninhabitable
91 25,000 homes and businesses, forced 200,000 people to evacuate and produced
92 massive power and transports outages for a total of 2.32 billion AUD of dam-
93 age (Foreign Policy, 2022). We will attribute this event to climate change using
94 dynamical systems theory to target the concurrent atmospheric circulation
95 patterns and search for pattern recurrences in the far (1948-1977) and recent
96 past (1990-2019). Our working hypothesis is that the far past acts as a coun-
97 terfactual world where the Earth climate was not influenced by anthropogenic
98 forcing when compared to the recent past (the factual world). Additionally,
99 we assume that 30 years is a long enough period to average out the interan-
100 nual variability of the atmospheric motions (as that caused, for example, by
101 El-Niño - Southern Oscillation). Finally we verify that these events produce
102 similar impacts on the targeted regions.

103 The paper is organized as follows: section 2 describes the data and methods
104 used in this study. This is followed by the presentation of the meteorology of
105 the event (Section 3) and by the results (Section 4) providing both a statistical
106 a dynamical attribution analysis. We conclude with a discussion and perspectives
107 in Section 5.

108 2 Data and Methods

109 2.1 Data

110 In order to detect significant changes in the circulation associated with Aus-
111 tralian Rain bombs, we use daily sea level pressure (*slp*), 500hPa geopotential
112 height (*z*500) and 2m air temperature (*t*2m) data from the NCEP/NCAR
113 reanalysis (Kalnay et al, 1996) over the period 01/01/1948 – 31/03/2022. The
114 data has a horizontal resolution of $2.5^\circ \times 2.5^\circ$.

115 The precipitation data are taken from the high resolution daily rainfall
 116 gridded datasets of the Bureau of Meteorology of Australia. The data has a
 117 horizontal resolution of $0.05^\circ \times 0.05^\circ$. Daily precipitation data from the Alderley
 118 station, close to Brisbane, is also used solely. For the ENSO index, we used
 119 the Nino3.4 detrended index.

120 2.2 Methods

121 Extreme Value Theory (EVT) has been introduced in the study of climate
 122 a decade ago (Freitas et al, 2008) and has gained a considerable amount of
 123 attention in both the applied mathematics and the climate science commu-
 124 nities (Lucarini et al, 2012, 2016; Faranda et al, 2019). It allows to compute
 125 recurrence times statistics for climatic systems, but also provides important
 126 information on the stability and the predictability of a particular climatic state.
 127 This information is contained in indicators that can be estimated via EVT-
 128 based methods, namely the instantaneous dimension D and the persistence Θ .
 129 The concept of instantaneous dimension is intuitive: for an atmospheric state
 130 ζ , e.g. a daily map of sea-level pressure on a given region, the instantaneous
 131 dimension $D(\zeta)$ measures the density of similar configurations. This implies
 132 that D can be related to both entropy and trajectory predictability. The sta-
 133 bility of the state ζ is measured by $\Theta(\zeta)$ defined as the average persistence time
 134 of trajectories around ζ . If ζ is a fixed point of the dynamics, $\Theta(\zeta) \rightarrow \infty$. For
 135 a trajectory immediately leaving the neighbourhood of $\Theta = 1$. In general, the
 136 more persistent the configuration, the more the system states will resemble ζ .

137 We can apply this framework to the study of weather extremes to study
 138 anthropogenic-driven climate change of weather patterns (Faranda et al, 2020).
 139 For each of the events, we identify the day where the largest impacts are
 140 detected. We then perform a visual inspection of the concurrent weather pat-
 141 tern. In most of the cases, we are interested in a synoptic object, i.e. a cyclone
 142 or anticyclone or a couple of these structures. During this identification, we
 143 select a region (a longitude/latitude box) that fits the synoptic map that we
 144 want to examine.

145 Once fixed the day of interest ζ we scan all the 3-days rolling averaged
 146 sea-level pressure slp and 500hPa geopotential $z500$ maps in two periods: 1948-
 147 1977 (counterfactual world) and 1990-2019 (factual world). For both periods
 148 we select the best 35 analogues (quantile 0.997) as the slp and $z500$ maps
 149 minimizing the pointwise euclidean distance with respect to the target ζ . The
 150 choice of a 30 years period for the factual and counterfactual periods ensures
 151 having a large statistical sample of slp and $z500$ maps to select authentic ana-
 152 logues and to satisfy both the assumptions of stationarity of the climate with
 153 respect to anthropogenic climate change while averaging over the interannual
 154 and interdecadal natural variability of the atmospheric circulation. Indeed, we
 155 have verified that the results do not depend sensibly on the choice of the num-
 156 ber of analogues provided that we extract between 25 and 50 analog maps.
 157 Once obtained the two sets of analogues for the factual and counterfactual
 158 periods, we average them out to search for significant differences Δslp and

159 $\Delta z500$. To determine significant changes, we apply a Welch's t-test (Welch,
160 1947) with different variance at each grid point. We mark as significant only
161 grid point changes for which the p -value of the test is below 0.05. Conditioning
162 to the dates determined for slp or $z500$ maps, we also study the associated 2
163 meters temperatures $t2m$ and total precipitation maps tp . The Welch's t-test
164 procedure is repeated on these ensembles to identify significant changes.

165 Using the framework of dynamical systems described above, we then intro-
166 duce few metrics to determine the recurrences properties of the map in the
167 counterfactual and factual world. This means that the metrics introduced
168 below are computed twice with respect to the analogues obtained in the two
169 periods.

- 170 • **Analog Quality Q :** we can study the typicality of ζ by comparing the
171 euclidean distance of ζ from its analogues with the distances of the analogues
172 from their own analogues. If the value of Q belongs to the same distribution
173 of the values of Q analogues, then typicality is ensured and attribution of
174 ζ can be performed. If instead the Q for the chosen day is larger than that
175 of the analog days, then this is an unprecedented slp or $z500$ configuration
176 and the results for attribution must be taken more carefully. A difference
177 in Q between the counterfactual and factual periods indicate a change in
178 typicality of the event due to climate change.
- 179 • **Predictability Index D :** we can compute the above defined dimension D of
180 the event ζ in both the periods to detect a climate-change induced shift in
181 predictability. Indeed, D is a proxy for the number of degrees of freedom
182 of the map, meaning that the higher the dimension the more unpredictable
183 the next slp or $z500$ maps will be. If the dimension D of the chosen day is
184 higher or lower than that of the analogues, then the day will be less or more
185 predictable than its closest dynamical situations.
- 186 • **Persistence Index Θ :** another information derived from the dynamical sys-
187 tems theory is the persistence of a given configuration. The persistence
188 counts for how many days we are likely to observe a map that is an analogs
189 of the one considered. Once again we will compute Θ for the two different
190 periods and using the analogs as well to detect shifts from the factual to the
191 counterfactual worlds.
- 192 • **Seasonality of Analog:** we can also simply count the number of analogs in
193 each month to detect whether a given circulation shifts towards earlier or
194 later months. This can have strong thermodynamic implications.

195 For more information, please refer to (Faranda et al, 2022).

196 We also provide results of the attribution conditional not on the past and
197 present climate, but on the El-Niño - Southern Oscillation (ENSO) mode.
198 ENSO is known to be a major factor in the variability of tropical and subtropi-
199 cal regions around the Pacific and likely played a role in the February 2022
200 event for which the mode was strongly negative. Therefore, we decided to run
201 the attribution analysis conditional on the Nino3.4 index being above the 75%

202 quantile (ENSO+) and below the 25% quantile (ENSO-) for the period 1948-
203 2019. Analogues are then computed in those two pools of data using either
204 3-days rolling averaged *slp* or *z500* maps.

205 **3 Meteorology and Impacts for the Australian** 206 **rain bombs**

207 In order to explain the rain bomb event, we identified two main ingredients: i)
208 an atmospheric river, formed north the continent around the 22nd of Febru-
209 ary, in the upper atmosphere – between eight and 10 kilometres up –, moved
210 from the ocean to the south reaching the continent and producing a contin-
211 uous flux of precipitation originating from the tropics, ii) a dipolar structure
212 consisting of a low pressure system in the coral Sea and a blocking anticyclone
213 further east. The combination of these elements allowed to transport moist
214 air from the tropics to the Coral sea and then condense the moisture that has
215 then fallen as rain thanks to the low pressure, and winds pushing rain over
216 Queensland’s south east. Precipitation was further enhanced by orographic
217 effects. At an even larger scale, the phenomena were embedded in a strong La
218 Nina phase, which induces additional air moisture in the south west Pacific
219 and wind circulation patterns that could have played a role in the intensity of
220 the event.

221 Preliminary results of the University of Melbourne reported by national and
222 international newspapers (see, e.g. [The Guardian \(2022\)](#)) showed that on the
223 26th and 27th of February, the two days with heaviest rain, 16 times the water
224 held by Sydney harbour (500 bn liters) flowed in the atmospheric river above
225 Queensland. Indeed during those days rainfall of over 400 millimetres was
226 recorded across the greater Brisbane area, summing up, for the 28th February
227 to a total of 676.8 millimetres of rainfall, the largest three, and seven, day total
228 ever recorded in Brisbane. Another record breaking amount of rainfall was
229 recorded in Mount Glorious which received rainfall in excess of 1770 millimetres
230 in the week until 28th of February. More than 30 locations across the south-
231 east recorded rainfall in excess of 1000 millimetres, resulting in the floods being
232 more intense than that of 1974. The unprecedented flooding that raised many
233 rivers above record highs moved south, leaving towns underwater. The area
234 of Sydney was more affected on the 3rd and the 8th of March with the city’s
235 chief reservoir, spilling at a rate in excess of 70 gigalitres a day on 3 March.
236 Residents in parts of western Sydney were told to evacuate for the second year
237 in a row as the city’s Warragamba Dam overflowed. But the system stalled
238 before it passed over Sydney.

239 Damage from floods is only partially estimated at this stage, but is expected
240 to reach almost AUD 2.3 billion ([Foreign Policy, 2022](#)), an estimate that
241 exceeds that of the Insurance Council of Australia, which also summed-up the
242 cost of claims from the disaster to AUD 1.45 billion ([ClimateCouncilAustralia,](#)
243 [2022](#)). This is somehow a lower bound as the estimates are expected to grow.

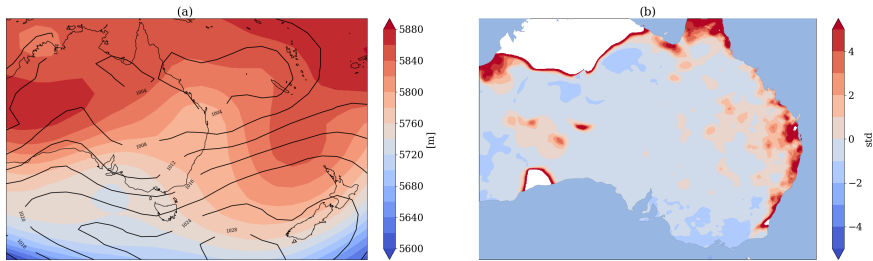


Fig. 1 Description of the rain bomb event. (a) Geopotential height at 500hPa (colors) and sea level pressure (contours) averaged over the 26th, 27th and 28th of February 2022. (b) Standardized anomaly of cumulated precipitation for the period 20th February - 20th March with respect to the 1990-2019 period. Regions in white correspond to standardized anomaly above 15 standard deviations.

244 Figure 1 (a) presents the synoptic situation averaged over the 26th, 27th
 245 and 28th of February over the region. We see the dipole structure with an
 246 upper level low pressure system centered above the Brisbane region and a high
 247 pressure system over the Coral sea. Figure 1 (b) presents the standardized
 248 anomaly of cumulated precipitations for a one month period (20/02-20/03)
 249 with respect to the 1990-2019 period. The Eastern coast of Australia saw
 250 extremely strong precipitations, with many locations exceeding 5 standard
 251 deviation anomalies with respect to climatology.

252 4 Results

253 4.1 Statistical attribution

254 To assess the change of probability of the event to climate change, we use the
 255 rapid statistical attribution method described in 2. We fit the 3-days rolling
 256 average precipitation yearly maxima in Alderley station to a Generalized
 257 Extreme Value (GEV) law for the factual and counterfactual periods.

258 Figure 2 shows the resulting GEV fit. In both the factual and counterfactual
 259 worlds the event of April 2022 was highly exceptional, with return periods of
 260 more than a thousand years. For high return periods, return levels are slightly
 261 higher in the counterfactual period, due to the January 1974 precipitation
 262 event that led to historical floods in Brisbane. However, the 95% confidence
 263 intervals are too wide to conclude to any detectable effect of climate change
 264 with this method.

265 Figure 3 shows the same analysis applied to the ENSO mode, using ENSO+
 266 as a factual period and ENSO- as a counterfactual period. Results show a
 267 much stronger effect of the la Niña phase (ENSO-) on precipitation rates in
 268 the Eastern Australian coast. The 2022 26th to 28th February event is very
 269 highly improbable during ENSO+ mode - with a return period of over 400
 270 years taking into account the 95% confidence interval - whereas it has a return
 271 period of 120 years according to the best estimation in ENSO- mode. This

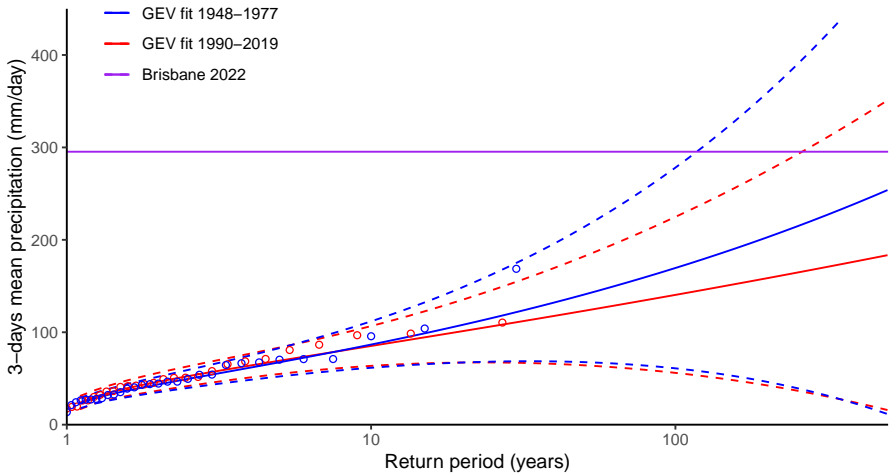


Fig. 2 Fit of the annual maximum of 3-days precipitation running means at Alderley station to a GEV in the factual and counterfactual periods. Gumbel plot of the GEV fit over 1948-1977 (blue lines with 95% uncertainty estimates), and 1992-2021 (red lines) using the maximum likelihood estimation. The purple line shows the value of intensity of the observed event at Alderley station in 2022.

272 is consistent with the influence of the strong la Niña phase currently ongoing
 273 on the intensity of the 2022 event suggested in 3. We however underline that
 274 the wide confidence intervals prevent again to obtain statistical significant
 275 differences at least at the 95% level chosen as a reference in this study.

276 4.2 Dynamical attribution

277 To identify the dynamical and thermodynamic factors which may have played
 278 a role in the intensity of the event, we ran the dynamical attribution framework
 279 presented previously.

280 Figures 4 and 5 present the results using respectively *slp* and *z500* analogues.
 281 These figures display the *slp/z500* (a-d), *t2m* (e-h) and *prate* (i-l)
 282 maps and, from left to right, the maps of the event (a,e,i), the composites of
 283 counterfactual (b,f,j) and factual (c,g,k) analogs and the difference between
 284 the factual and counterfactual analogs (d,h,l) where hashed-filled areas show
 285 significant differences. Distributions of additional metrics comparing the
 286 counterfactual and factual periods, namely analogs quality, predictability,
 287 persistence and distribution by season are shown in panels m-p, respectively.

288 For the *slp* analogues, we firstly notice that the analogues quality is not
 289 good and therefore results must be interpreted carefully (panel (m)). In the
 290 factual period, there is a signal of intensified high-pressures over New Zealand,
 291 which may be related to the stronger advection of moist air from the Coral
 292 sea. When we look at the precipitation difference map (Fig. 4 (l)), there are
 293 indeed stronger precipitations on the Eastern coast of Australia in the factual

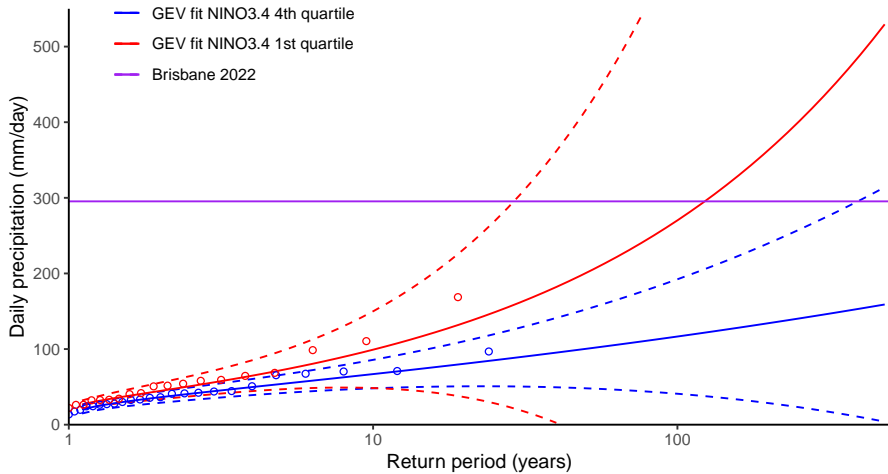


Fig. 3 Fit of the annual maximum of 3-days precipitation running means at Alderley station to a GEV, depending on El Niño 3.4 detrended index. Gumbel plot of the GEV fit over years in the 1st quartile (red lines) and 4th quartile (blue lines) of NINO3.4 index average over JFM from 1944 to 2021, with 95% uncertainty estimates. The purple line shows the value of intensity of the observed event at Alderley station in 2022.

294 period but only few regions are significantly different than the counterfactual
 295 period and do not fully correspond to the regions where the precipitations
 296 are maximum during the February 2022 event. There is moreover no strong
 297 thermodynamic signal as depicted in panel (h) using 2m air temperature which
 298 does not display significant differences between the factual and counterfactual
 299 periods on the Eastern coast and in the Coral sea. However, panel (o) and (p)
 300 show that the predictability is lower and the persistence is higher in the factual
 301 period. The event is particularly persistent compared to its analogues in the
 302 factual period which may explain the intensity of the event.

303 This results are confirmed when using the $z500$ analogues (Fig. 5), which
 304 are better as shown in panel (m). The factual period displays stronger high
 305 $z500$ over the northern region but also almost no significant thermodynamic
 306 signal (panel (h)). The low predictability (panel (n)) but high persistence
 307 (panel (p)) of the event is also noticed using $z500$ analogues. When it comes to
 308 precipitations, even though they are stronger during the factual period (panel
 309 (l)), this difference is not significant.

310 These results are coherent with the statistical attribution in so far as the
 311 thermodynamic signal associated with climate change is weak. There is how-
 312 ever a noticeable dynamical signal in the two periods as represented in the slp
 313 and $z500$ analogues difference maps. One may indeed notice that ENSO, which
 314 is the major driver of variability in the region, was in a strong and persistent
 315 La Nina phase during the event, which is not fully represented using analogues
 316 (see figure 6). We therefore decided to run the same dynamical attribution

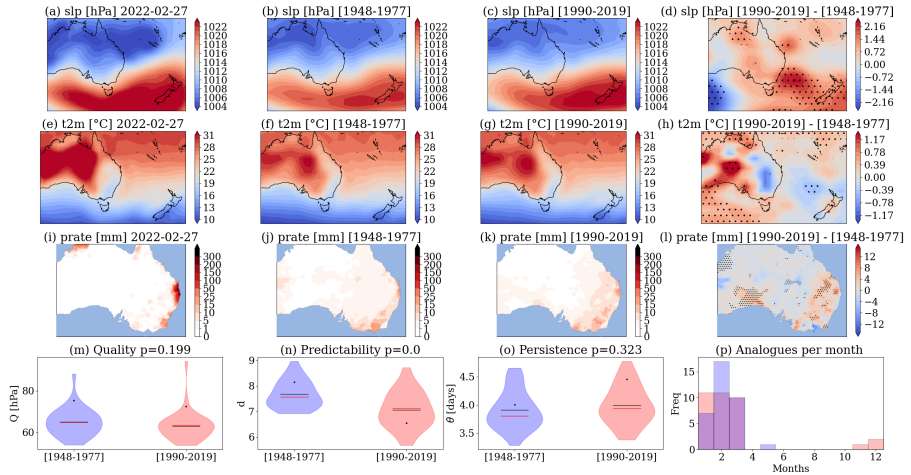


Fig. 4 Dynamical attribution using *slp* analogues for the Australian rain bomb on 27-02-2022. 3-days rolling mean sea-level pressure *slp* (a), 2-meter temperatures *t2m* (e) and total precipitation *prate* (i) centered on the 27-02-2022. Average of the 35 sea-level pressure analogs found for the counterfactual [1948-1977] (b) and factual [1990-2019] (c) periods and corresponding 2-meter temperatures (f,g) and daily precipitation rate (j,k). Δslp (d), $\Delta t2m$ (h) and $\Delta prate$ (l) between factual and counterfactual periods: hashed-filled areas show significant differences. Violin plots for counterfactual (blue) and factual (red) periods for the Analogues Quality Q (m) the Predictability index D (n), the Persistence index θ (o) and the distribution of analogs in each month (p). Values for the selected day are marked by a black dot.

317 analysis using the Nino3.4 index to define counterfactual (ENSO-) and factual
 318 (ENSO+) periods.

319 The results of this analysis are presented in figures 7 and 8 using respec-
 320 tively *slp* and *z500* analogues. On the dynamical side, there is a significant
 321 stronger upper level low during ENSO- phase (Fig. 8 panel (d)) analogues.
 322 Using both analogues, the thermodynamic signal is much stronger during
 323 ENSO+ events, which may explain the absence of signal when doing the analy-
 324 sis during past and present periods: the natural variability is stronger than the
 325 climate change signal on this region. When it comes to precipitations, there is
 326 a strong positive signal on the Eastern coast and Brisbane regions during La
 327 Nina phases using *slp* analogues but the quality of analogues is low and these
 328 results are not significant using *z500* analogues.

329 5 Conclusions

330 In this paper we have performed a statistical and dynamical attribution of the
 331 Australian rain bomb event of February 2022. We have used both reanalyses
 332 and historical records of daily precipitations in the past (1948-1977, coun-
 333 terfactual) and present (1990-2019, factual) periods. From a statistical point
 334 of view, this extreme precipitation event was unprecedented in the Brisbane

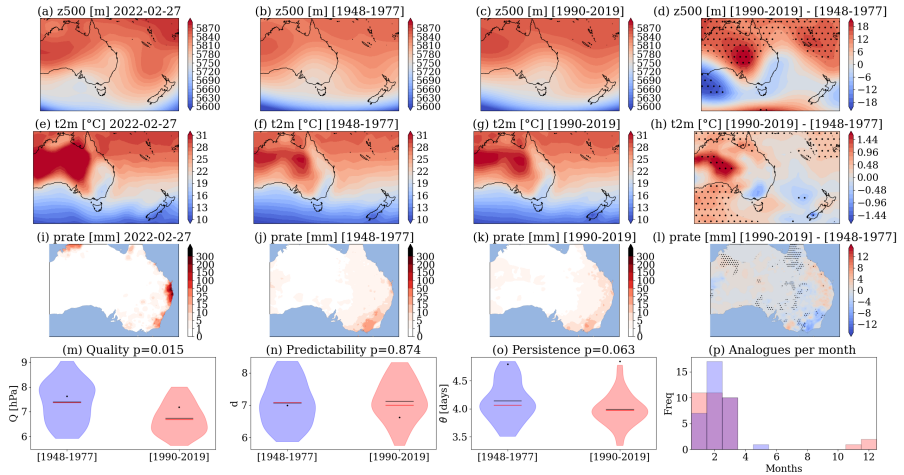


Fig. 5 Dynamical attribution using $z500$ analogues for the Australian rain bomb on 27-02-2022. 3-days rolling mean 500hPa geopotential height $z500$ (a), 2-meter temperatures $t2m$ (e) and total precipitation $prate$ (i) centered on the 27-02-2022. Average of the 35 500hPa geopotential height analogs found for the counterfactual [1948-1977] (b) and factual [1990-2019] (c) periods and corresponding 2-meter temperatures (f,g) and daily precipitation rate (j,k). $\Delta z500$ (d), $\Delta t2m$ (h) and $\Delta prate$ (i) between factual and counterfactual periods: hashed-filled areas show significant differences. Violin plots for counterfactual (blue) and factual (red) periods for the Analogs Quality Q (m) the Predictability index D (n), the Persistence index θ (o) and the distribution of analogs in each month (p). Values for the selected day are marked by a black dot.

335 region and very intense with regards to historical records in the broader East-
 336 ern coast of Australia. The statistical attribution suggests that this event has
 337 a low probability to happen both in the past and present climate (less than
 338 one in a century). There is no clear signal of a climate change influence (high
 339 uncertainty) which translates in a low evidence for the attribution of this event
 340 to climate change.

341 The dynamical attribution, performed using the method of analogues cir-
 342 culation patterns proposed in Faranda et al (2022) to those observed during
 343 the events suggest the exceptional characteristics of the event which appears
 344 to be unprecedented in both the factual and counterfactual distributions of
 345 weather patterns: it has arisen as the combination of ingredients: the tropical
 346 moisture was deflected to the subtropics, collected and lifted by a low pressure
 347 system blocked by an high pressure offshore the Coral sea. This combination
 348 created an atmospheric river capable of transporting several gegaliters of water
 349 towards the Queensland and the South West of the continent. Finally, La Niña
 350 phase of the El-Niño-Southern-Oscillation likely played a significant role in the
 351 intensity of the event.

352 The main limitation of this study is that we do not use climate models:
 353 the rational for doing so comes from the evidence that both large, regional

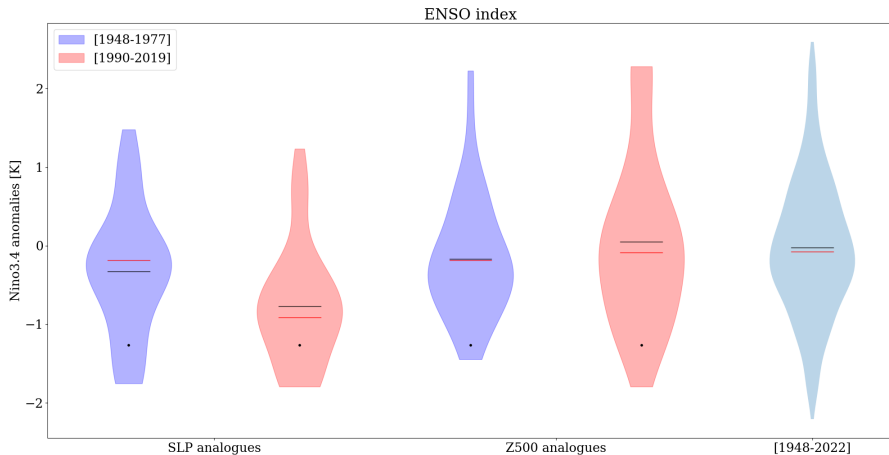


Fig. 6 Distribution of ENSO index between factual and counterfactual periods for the two types of analogues. Blue (resp. red) violin plots represent the distribution of the ENSO index for the analogues in the counterfactual (resp. factual) period. The red (resp. black) line depicts the median (resp. mean) of the distribution. The black dot corresponds to the value of the ENSO index during the February 2022 event. The last violin plot depicts the distribution of the ENSO index for all dates between 1948 and 2019.

354 and local phenomena contributed to this event. In order to perform an attribution
 355 study based on models, we would need a large ensemble of convection
 356 permitting models resolving at least the region shown in Fig. 1, with specific
 357 runs capable to evaluate also the contribution of la Nina to the event. Even
 358 with such models, the detailed physics of the precipitation could still depend
 359 on the microphysics introduced in the model as shown by Ban et al (2021).
 360 A further limitation of this study is the use of factual and counterfactual peri-
 361 ods consisting of only 30 years. While we could in principle consider the whole
 362 period twice, as in the protocol described by Philip et al (2020), we cannot
 363 here use the implicit assumption of stationarity of the variability of the rain-
 364 fall extremes that is underlying the protocol. While this is a limitation on the
 365 available data, it is a fair way to account for the variability of extremes, allow-
 366 ing for a larger uncertainty and a conservative estimates on the role of climate
 367 change to triggering this event.

368 To frame our results in a more general framework, we observe that they
 369 are in line with what the IPCC report AR6, WG1, Chapter 11.4, states about
 370 rainfall over the region, namely that “Available evidence has not shown an
 371 increase or a decrease in heavy precipitation over Australasia as a whole
 372 (medium confidence), but heavy precipitation tends to increase over North-
 373 ern Australia (particularly the north-west) and decrease over the eastern and
 374 southern regions.” (Seneviratne et al, 2021) . We however observe that the
 375 compounding dynamical elements driving this event are also observed in a
 376 series of unprecedented extreme weather events occurred in the last few years,
 377 including the 2021 Canada heat dome, the Antarctica atmospheric rivers, the

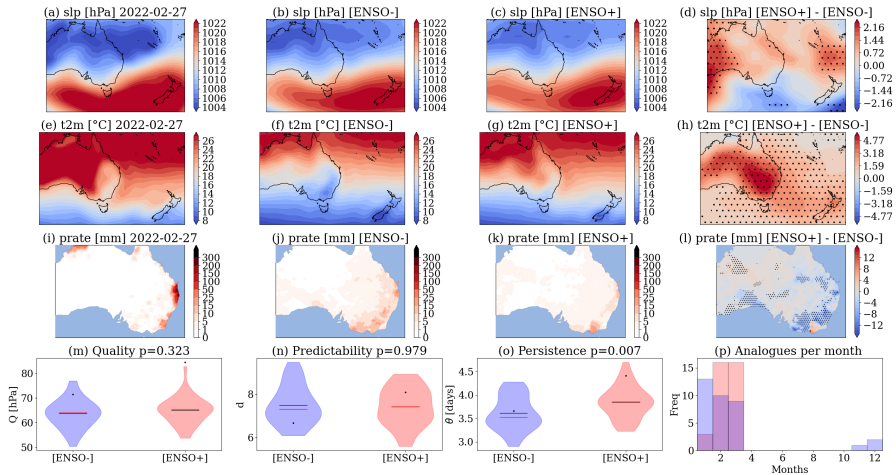


Fig. 7 Dynamical attribution using *slp* analogues for the Australian rain bomb on 27-02-2022 relative to the ENSO index. 3-days rolling mean 500hPa geopotential height $z500$ (a), 2-meter temperatures $t2m$ (e) and total precipitation $prate$ (i) centered on the 27-02-2022. Average of the 35 sea-level pressure analogs found for the counterfactual [ENSO-] (b) and factual [ENSO+] (c) periods and corresponding 2-meter temperatures (f,g) and daily precipitation rate (j,k). $\Delta z500$ (d), $\Delta t2m$ (h) and $\Delta prate$ (i) between factual and counterfactual periods: hashed-filled areas show significant differences. Violin plots for counterfactual (blue) and factual (red) periods for the Analogs Quality Q (m) the Predictability index D (n), the Persistence index θ (o) and the distribution of analogs in each month (p). Values for the selected day are marked by a black dot.

378 2022 Indian, Chinese, Western European and North American heatwaves. Such
 379 series of record breaking events raise the question of the emergence of new phe-
 380 nomena linked to global warming, a field to explore statistically, e.g. by using
 381 the concept of time of emergence introduced in Hawkins and Sutton (2012)
 382 and dynamically, e.g. by looking the possible presence of tipping elements in
 383 the climate system (Lenton et al, 2008).

384 **Acknowledgments.** We acknowledge the Bureau of Meteorology of Aus-
 385 tralia for their help in obtaining the high resolution daily rainfall gridded
 386 datasets. The authors acknowledge the support of the INSU-CNRS-LEFE-
 387 MANU grant (project DINCLIC), as well as the gran ANR-19-ERC7-0003
 388 (BOREAS). This work has received support from the European Union's Hori-
 389 zon 2020 research and innovation programme under grant agreement No.
 390 101003469 (XAIDA) and the Marie Skłodowska-Curie grant agreement No.
 391 956396 (EDIPI).

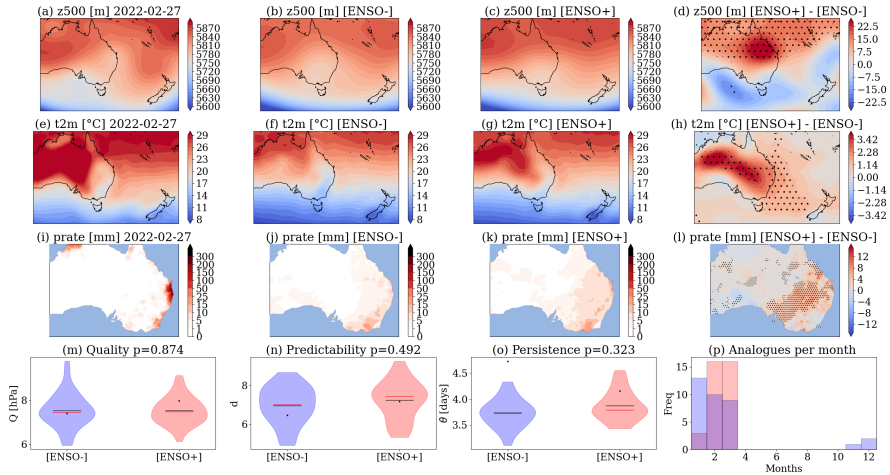


Fig. 8 Dynamical attribution using $z500$ analogues for the Australian rain bomb on 27-02-2022 relative to the ENSO index. 3-days rolling mean 500hPa geopotential height $z500$ (a), 2-meter temperatures $t2m$ (e) and total precipitation $prate$ (i) centered on the 27-02-2022. Average of the 35 500hPa geopotential height analogs found for the counterfactual [ENSO-] (b) and factual [ENSO+] (c) periods and corresponding 2-meter temperatures (f,g) and daily precipitation rate (j,k). $\Delta z500$ (d), $\Delta t2m$ (h) and $\Delta prate$ (i) between factual and counterfactual periods: hashed-filled areas show significant differences. Violin plots for counterfactual (blue) and factual (red) periods for the Analogs Quality Q (m) the Predictability index D (n), the Persistence index θ (o) and the distribution of analogs in each month (p). Values for the selected day are marked by a black dot.

392 Declarations

- 393 • Funding: This project has received funding from the European Union's Hori-
 394 zon 2020 research and innovation programme under the Marie Skłodowska-
 395 Curie grant agreement N° 956396 under grant agreement No. 101003469
 396 (XAIDA).
- 397 • Conflict of interest: The authors declare no conflict of interest.
- 398 • Ethics approval: Not applicable.
- 399 • Consent to participate: Not applicable.
- 400 • Consent for publication: Not applicable.
- 401 • Availability of data and materials: NCEP data are available on the
 402 NOAA website at <https://psl.noaa.gov/data/gridded/data.ncep.reanalysis.html>. Rainfall data over Australia are available at the National Computa-
 403 tional Infrastructure (NCI) THREDDS server at <https://dapds00.nci.org.au/thredds/catalog/zv2/agcd/v1/precip/total/r005/01day/catalog.html>.
- 404 • Code availability: The main results of this work were obtained using Python.
 405 The scripts are available upon request.
- 406 • Authors' contributions: CC, NM and RN performed the analysis. DF
 407 designed the analyses. All authors participated to the manuscript prepara-
 408 tion and writing.
 409
 410

References

- 411
- 412 Abram NJ, Henley BJ, Sen Gupta A, et al (2021) Connections of climate
413 change and variability to large and extreme forest fires in southeast australia.
414 *Communications Earth & Environment* 2(1):1–17
- 415 Ban N, Caillaud C, Coppola E, et al (2021) The first multi-model ensemble of
416 regional climate simulations at kilometer-scale resolution, part i: evaluation
417 of precipitation. *Climate Dynamics* 57(1):275–302
- 418 Borchers Arriagada N, Palmer AJ, Bowman DM, et al (2020) Unprecedented
419 smoke-related health burden associated with the 2019–20 bushfires in eastern
420 australia. *Medical Journal of Australia* 213(6):282–283
- 421 Canadell JG, Meyer C, Cook GD, et al (2021) Multi-decadal increase of forest
422 burned area in australia is linked to climate change. *Nature communications*
423 12(1):1–11
- 424 Church JA, Hunter JR, McInnes KL, et al (2006) Sea-level rise around the
425 australian coastline and the changing frequency of extreme sea-level events.
426 *Australian Meteorological Magazine* 55(4):253–260
- 427 Church JA, McInnes KL, Monselesan D, et al (2017) Sea level rise and
428 allowances for coastal councils around australia—guidance material
- 429 ClimateCouncilAustralia (2022) A supercharged climate:
430 Rain bombs, flash flooding and destruction. Avail-
431 able at [https://www.climatecouncil.org.au/resources/
432 supercharged-climate-rain-bombs-flash-flooding-destruction](https://www.climatecouncil.org.au/resources/supercharged-climate-rain-bombs-flash-flooding-destruction) Accessed:
433 08/07/2022
- 434 Cook BI, Mankin JS, Anchukaitis KJ (2018) Climate change and drought:
435 From past to future. *Current Climate Change Reports* 4(2):164–179
- 436 Dey R, Lewis SC, Arblaster JM, et al (2019) A review of past and projected
437 changes in australia’s rainfall. *Wiley Interdisciplinary Reviews: Climate*
438 *Change* 10(3):e577
- 439 Douville H, Raghavan K, Renwick J, et al (2021) Water Cycle Changes. In
440 *Climate Change 2021: The physical science basis. contribution of Working*
441 *Group I to the Sixth Assessment Report of the Intergovernmental Panel on*
442 *Climate Change*
- 443 Faranda D, Alvarez-Castro MC, Messori G, et al (2019) The hammam effect or
444 how a warm ocean enhances large scale atmospheric predictability. *Nature*
445 *communications* 10(1):1–7

- 446 Faranda D, Vrac M, Yiou P, et al (2020) Changes in future synoptic circulation
447 patterns: consequences for extreme event attribution. *Geophysical Research*
448 *Letters* 47(15):e2020GL088,002
- 449 Faranda D, Bourdin S, Ginesta M, et al (2022) A climate-change attribution
450 retrospective of some impactful weather extremes of 2021. *Weather and*
451 *Climate Dynamics Discussions* pp 1–37
- 452 Filkov AI, Ngo T, Matthews S, et al (2020) Impact of australia’s catastrophic
453 2019/20 bushfire season on communities and environment. retrospective
454 analysis and current trends. *Journal of Safety Science and Resilience*
455 1(1):44–56
- 456 Foreign Policy (2022) The ‘rain bomb’ that could shape the aus-
457 tralian election. Available at [https://foreignpolicy.com/2022/03/11/
458 australia-flood-election-climate-change/](https://foreignpolicy.com/2022/03/11/australia-flood-election-climate-change/) Accessed: 08/07/2022
- 459 Freitas ACM, Freitas JM, Todd M (2008) Hitting time statistics and extreme
460 value theory. [0804.2887](https://doi.org/10.1007/s10992-008-9084-7)
- 461 Grainger S, Fawcett R, Trewin B, et al (2022) Estimating the uncertainty
462 of australian area-average temperature anomalies. *International Journal of*
463 *Climatology* 42(5):2815–2834
- 464 Hawkins E, Sutton R (2012) Time of emergence of climate signals. *Geophysical*
465 *Research Letters* 39(1)
- 466 Head L, Adams M, McGregor HV, et al (2014) Climate change and australia.
467 *Wiley Interdisciplinary Reviews: Climate Change* 5(2):175–197
- 468 Hirabayashi Y, Mahendran R, Koirala S, et al (2013) Global flood risk under
469 climate change. *Nature climate change* 3(9):816–821
- 470 Hobday AJ, Pecl GT, Fulton B, et al (2018) Climate change impacts,
471 vulnerabilities and adaptations: Australian marine fisheries
- 472 Holland MM, Smith JA, Everett JD, et al (2020) Latitudinal patterns in
473 trophic structure of temperate reef-associated fishes and predicted conse-
474 quences of climate change. *Fish and Fisheries* 21(6):1092–1108
- 475 Jetten J, Fielding KS, Crimston CR, et al (2021) Responding to climate
476 change disaster: The case of the 2019/2020 bushfires in australia. *European*
477 *Psychologist* 26(3):161
- 478 Kalnay E, Kanamitsu M, Kistler R, et al (1996) The ncep/ncar 40-year reanal-
479 ysis project. *Bulletin of the American meteorological Society* 77(3):437–472

480 Lenton TM, Held H, Kriegler E, et al (2008) Tipping elements in the
481 earth's climate system. *Proceedings of the national Academy of Sciences*
482 105(6):1786–1793

483 Lucarini V, Faranda D, Wouters J (2012) Universal behaviour of extreme value
484 statistics for selected observables of dynamical systems

485 Lucarini V, Faranda D, Freitas ACM, et al (2016) Extremes and recurrence in
486 dynamical systems. [1605.07006](https://doi.org/10.1007/s11069-016-0700-6)

487 Masson-Delmotte V, Zhai P, Pirani A, et al (2021) Ipcc The physical science
488 basis. contribution of working group I to the Sixth Assessment Report of
489 the Intergovernmental Panel on Climate Change

490 Philip S, Kew S, van Oldenborgh GJ, et al (2020) A protocol for probabilis-
491 tic extreme event attribution analyses. *Advances in Statistical Climatology,*
492 *Meteorology and Oceanography* 6(2):177–203

493 Seneviratne S, Zhang X, Adnan M, et al (2021) Weather and climate extreme
494 events in a changing climate. In *Climate Change 2021: The physical science*
495 *basis. contribution of Working Group I to the Sixth Assessment Report of*
496 *the Intergovernmental Panel on Climate Change*

497 The Guardian (2022) ‘this is an emergency’: Australia’s extreme
498 weather crises spark anger at climate inaction. Available
499 at [https://www.theguardian.com/australia-news/2022/apr/09/
500 this-is-an-emergency-australias-extreme-weather-crisis-spark-anger-at-climate-inaction](https://www.theguardian.com/australia-news/2022/apr/09/this-is-an-emergency-australias-extreme-weather-crisis-spark-anger-at-climate-inaction)
501 Accessed: 08/07/2022

502 The New Daily (2022) ‘very unusual’: Australia’s east coast cities are feeling
503 their coldest start to winter in decades. Available at [https://thenewdaily.
504 com.au/news/national/2022/06/09/cold-winter-weather-australia](https://thenewdaily.com.au/news/national/2022/06/09/cold-winter-weather-australia)
505 Accessed: 08/07/2022

506 Ukkola AM, De Kauwe MG, Roderick ML, et al (2020) Robust future
507 changes in meteorological drought in cmip6 projections despite uncertainty
508 in precipitation. *Geophysical Research Letters* 47(11):e2020GL087,820

509 Welch BL (1947) The generalization of ‘student’s’problem when several
510 different population variances are involved. *Biometrika* 34(1-2):28–35

511 Wilby RL, Keenan R (2012) Adapting to flood risk under climate change.
512 *Progress in physical geography* 36(3):348–378

513 Wolff NH, Mumby PJ, Devlin M, et al (2018) Vulnerability of the great barrier
514 reef to climate change and local pressures. *Global change biology* 24(5):1978–
515 1991

⁵¹⁶ Woodruff JD, Irish JL, Camargo SJ (2013) Coastal flooding by tropical
⁵¹⁷ cyclones and sea-level rise. *Nature* 504(7478):44–52